

The photolysis of colloidal iron in the oceans

Mark L. Wells*†, Lawrence M. Mayer†,
Olivier F. X. Donard‡, Marta M. de Souza Sierra‡
& Steve G. Ackelson§

† Department of Oceanography, University of Maine,
Darling Marine Center, Walpole, Maine 04573, USA

‡ Laboratoire de Photophysique et Photochimie Moleculaire,
Universite de Bordeaux I, 33405 Talence Cedex, France

§ Bigelow Laboratory for Ocean Sciences, McKown Point,
W. Boothbay Harbor, Maine 04575, USA

THE extent to which iron limits primary production in open ocean waters depends not only on the aeolian supply^{1–3}, but also on factors that control its availability for biological uptake. Although the marine chemistry of iron is poorly understood, much of it occurs in refractory particulate^{1,2} and colloidal⁴ states—forms unavailable for direct assimilation by phytoplankton^{5,6}. But iron availability depends on its chemical lability⁵, or ease of dissolution; hence processes that alter the lability of particulate and colloidal iron in sea water govern their availability to phytoplankton. Here we report that light increases the lability of colloidal iron in sea water of pH 8, with a photon-normalized spectral dependence that generally increases with decreasing wavelength from 400–300 nm. From optical modelling we predict that the incident solar spectrum, combined with the preferential attenuation of shorter ultraviolet wavelengths in sea water, will lead to a maximum depth-integrated photoreaction near 380–400 nm. Our results show that the photolysis of forms of solid iron may occur deep into the ocean's euphotic zone, and hence that the availability of iron to phytoplankton in the ocean may be much greater than previously thought.

Phytoplankton obtain iron by forming complexes of dissolved Fe(III) hydroxy species at membrane-bound uptake sites, followed by transport into the cell^{7,8}. Iron availability is therefore a function of the replenishment rate of Fe(III) hydroxy species to solution, in other words the dissolution kinetics, or chemical lability, of colloidal and particulate iron^{5,6}. The chemical lability of iron in sea water can be determined by reaction with the complexing agent 8-hydroxyquinoline (oxine); oxine-iron complexes formed in solution are extracted onto C₁₈ resin and the iron measured after elution by graphite furnace atomic absorption spectrometry⁵. There is a strong positive correlation between the fraction of iron complexed by oxine and the growth rates of marine algae in cultures, demonstrating that the reactivity of iron to form complexes with algal membrane transport ligands is covariant with its reactivity with chelators such as oxine⁵. Sunlight increases the oxine reactivities of both poorly crystalline ferrihydrites and the highly crystalline oxyhydroxide goethite in sea water⁹. (Goethite is one of the most stable of the iron oxyhydroxides and is widespread in terrestrial and marine systems.) This photoprocess apparently proceeds through a cycle of photoreductive dissolution/rapid reoxidation/precipitation involving organic chromophores, and yields amorphous, highly labile Fe(III) precipitates⁹ (Fe²⁺ is a transient species¹⁰ in oxic sea water of pH 8). But the oceanographic relevance of this photochemical cycling of iron largely depends on the spectral dependence of the photoreaction, which controls the penetration of iron photolysis into the euphotic zone.

We determined the photo-induced changes in iron lability at different wavelengths of ultraviolet and visible light by spiking sea water with colloidal iron of low lability and measuring its oxine reactivity after irradiation. We used surface sea water (5 m) from the Damariscotta estuary (Maine, USA), shelf water

(30 m) 30 km off the Gironde river estuary (France), and surface water (45 m) from the eastern margin of the Weddell Sea, Antarctica (75° 21.1' S, 25° 48.8' W). All seawater samples were collected using clean techniques that avoided contamination from the surface microlayer. Measurements of seawater absorbance and corrected¹¹ fluorescence spectra showed similar spec-

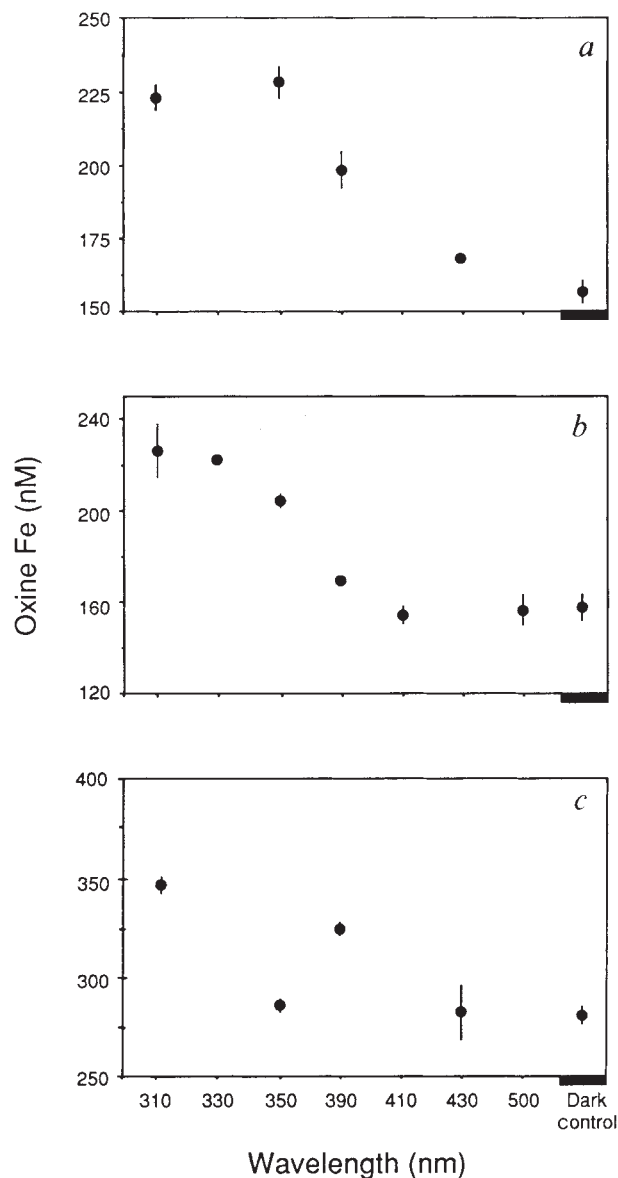


FIG. 1 The extent of photoreaction in 5 min of 90° FERR at different wavelengths in *a*, sea water from the Damariscotta river estuary, *b*, sea water off the Gironde River estuary and *c*, Antarctic sea water. Freshly prepared 90° FERR (see text) was added to the different sea waters (4 μM ferrihydrite) and irradiated in quartz-windowed, 10-cm spectrophotometer cells with an electric arc light source. Light was filtered through an adjustable monochromator to give 10 nm bandwidths centred at various ultraviolet and visible wavelengths. Solution temperatures were maintained at 9.5 ± 0.5 °C during irradiation. After irradiation, oxine was added to the cells and incubated for one hour at pH 6 (22 °C) before extracting the oxine-iron complexes from duplicate subsamples onto C₁₈ columns. The columns were then eluted with methanol and the iron determined by graphite furnace atomic absorption. Complete details of the methodology are given in Wells *et al.*⁵. The mean and range of duplicate analyses are shown. The detection limit was 50 nM iron with a precision of ±10%. The differences in the oxine reactivity of 90° FERR among the dark controls were probably due to minor temperature differences in iron stock before heating to 90 °C. Light intensities were measured at the specific irradiation wavelengths by chemical actinometry¹⁶; the changes in iron lability shown here are normalized to photon flux.

* Present address: Marine Research Division, A-020, Scripps Institution of Oceanography, University of California, San Diego, La Jolla, California 92093, USA.

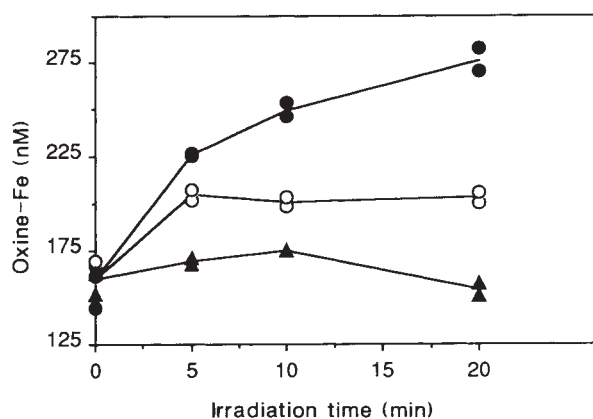


FIG. 2 Photoinduced changes in the oxine reactivity of 90° FERR in Gironde sea water. Freshly prepared 90° FERR (see text) was added to Gironde sea water (4 μM ferrihydrite) and irradiated at 310 nm (●), 350 nm (○) and 390 nm (▲). The irradiation conditions were as described in Fig. 1. The changes in iron lability shown here are normalized to photon flux.

tral patterns but decreasing intensities (and therefore organic concentrations) in the order Damariscotta > Gironde > Antarctic. The iron substrate used in these experiments was synthetic colloidal ferrihydrite produced by heating freshly precipitated ferrihydrite at 90 °C for 5 min (90° FERR³). This ferrihydrite was selected because it is relatively unavailable to phytoplankton⁵, its chemical lability is similar to measured values of particulate iron lability in coastal and offshore sea waters¹², and its lability remains constant in the dark⁹.

Irradiation increased the oxine reactivity of 90° FERR in each of the three sea waters, the photolysis intensifying with decreasing ultraviolet wavelengths below 400 nm but absent at higher (photosynthetically active) wavelengths during the 5-min irradiation (Fig. 1). This wavelength dependence is very similar to that for the photoproduction of free radicals in surface sea water, which are short-lived intermediaries in marine photochemical transformations¹³. The iron photoreaction persisted longer at shorter wavelengths (Fig. 2). Pre-irradiating the seawater with strong ultraviolet light eliminated the photoreaction

(not shown), suggesting that the reaction, and its wavelength dependence, was caused by organic chromophores. These chromophores probably form surface complexes on iron oxyhydroxides and cause ligand-to-metal charge transfers on photooxidation. Continuing photolysis presumably requires the sustained adsorption of new chromophores from solution. There were only slight changes in seawater absorbance (230–600 nm) or fluorescence spectra (emission scans of 320–600 nm with excitation at 313 and 370 nm) during the photoreaction experiments, and no clear losses of identifiable chromophores or fluorophores were detected as a result of the narrow-band irradiations that we used. The nature and direct source of the organic chromophores involved in iron photolysis are therefore unknown.

The photon-normalized reaction rates measured here are probably not representative of natural conditions; wavelength-specific photon fluxes were 10 to 100 times greater than for natural sunlight. This should cause faster photodegradation of the organic chromophores, and thus more rapid cessation of the photoreaction. In addition, the concentrations of 90° FERR added were two to three orders of magnitude higher than found in coastal and open ocean waters, respectively. The resultant, unrealistically high iron:chromophore ratios possibly lead to underestimation of the rate and extent of iron photolysis. More detailed studies of the photolysis kinetics of 90° FERR and colloidal goethite with simulated and natural sunlight are reported elsewhere⁹. In any event, the relative changes in 90° FERR lability over short (5-min) irradiation intervals (Fig. 1) demonstrate a spectral dependence for the photoreaction that is qualitatively similar among these diverse environments, and suggest that iron photolysis occurs commonly in surface waters.

The depth distribution of the relative rate of iron photolysis in sea water was modelled using the 5-min, photon-specific reaction rates of 90° FERR (Fig. 1) and the calculated, downwelling, diffuse irradiance in sea water. We modelled two water types having optical properties typical of coastal and open ocean waters; the sole difference between these being the extent of light attenuation due to organic matter. The resultant light fields were combined with the Damariscotta photolysis data in Fig. 1a. The Damariscotta data can be used to obtain a reasonable first approximation of colloidal iron photolysis in open ocean conditions because photolysis rate constants of 90° FERR in Damariscotta and Sargasso sea water under normal sunlight are nearly identical⁹. Our model does not account for the depth

Relative oxine-Fe production
(10^{-14} mol m⁻² s⁻¹)

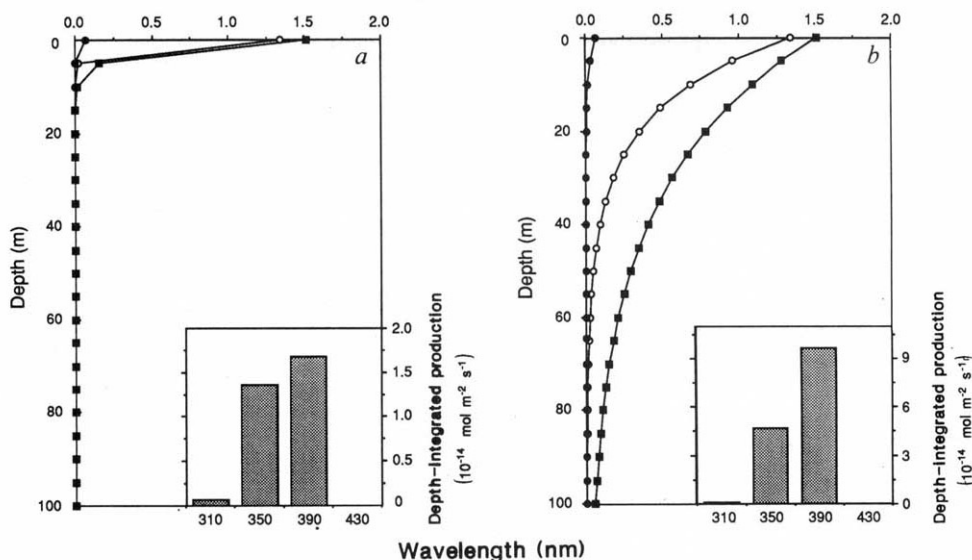


FIG. 3 The relative depth dependence of colloidal iron photolysis in a, coastal and b, open ocean sea water calculated from the photon-specific reaction rates and the estimated downwelling diffuse irradiance at 310 nm (●), 350 nm (○) and 390 nm (■). The optical model was constructed using mid-day, mid-latitude solar irradiances at sea level under a clear sky¹⁷. To determine the in-water diffuse attenuation coefficients at these wavelengths, we summed absorption coefficients for clear water¹⁸ and gelbstoff¹⁹ and light scattering due to clear water¹⁸. The relative oxine-iron photoproduction rates with depth were calculated as the product of the 5-min photon-specific photolysis rate of 90° FERR determined from Fig. 1a and the calculated vertical distribution of photon flux²⁰.

dependence of chromophore concentrations or any other depth or site-specific factor that might affect rate or extent of photo-reaction.

From the model results, as relative photoproduction rates of oxine-reactive iron (Fig. 3), we predict that colloidal iron photolysis would be concentrated in the upper 5–10 m in coastal waters, but would occur to depths >100 m in open ocean waters. In the open ocean, then, iron photolysis may operate over much of the depth range of photosynthetically active phytoplankton. Although these rate data must be considered to be preliminary (the light source and iron concentrations in these experiments were substantially different from natural conditions) the predicted depth distribution of iron photolysis closely matches the newly measured Fe(II) abundance in profiles of clear ocean water¹⁴. The depth-integrated production shows a reversal in the relative importance of wavelengths; substantially more colloidal iron photolysis would be associated with wavelengths near 390 nm than near 310 nm because of the lower incident spectral abundance and higher in-water attenuation of shorter ultraviolet wavelengths. Concentrations of chromophores that are activated by longer ultraviolet wavelengths (350–400 nm) are then likely to be the important cause of iron photolysis in sea water. Incubation experiments testing for iron limitation in sea water therefore should be conducted in containers that reproduce the ambient ultraviolet light conditions for the depth of interest.

Our experimental data and optical modelling, in conjunction with other experiments showing that highly crystalline Fe(III)

oxhydroxides such as goethite also are photolabile⁹, support the hypothesis that the photolysis of colloidal and particulate iron extends deep into the euphotic zone in open ocean environments. The availability of iron therefore may be much greater than estimated by the simple chemical dissolution of iron from particulates such as aeolian dust. □

Received 31 January; accepted 29 July 1991.

1. Martin, J. H. & Fitzwater, S. E. *Nature* **331**, 341–343 (1988).
2. Martin, J. H. & Gordon, R. M. *Deep Sea Res.* **35**, 177–196 (1988).
3. Martin, J. H., Gordon, R. M., Fitzwater, S. & Broenkow, W. W. *Deep Sea Res.* **36**, 649–680 (1989).
4. Mill, A. J. B. *Envir. Tech. Lett.* **1**, 97–108 (1980).
5. Wells, M. L., Mayer, L. M. & Guillard, R. R. L. *Mar. Chem.* **33**, 23–40 (1991).
6. Rich, H. W. & Morel, F. M. M. *Limnol. Oceanogr.* **35**, 652–662 (1990).
7. Anderson, M. A. & Morel, F. M. M. *Limnol. Oceanogr.* **27**, 789–813 (1982).
8. Morel, F. M. M. & Hudson, R. J. M. in *Chemical Processes in Lakes* (ed. Stumm, W.) 251–281 (Wiley, New York, 1985).
9. Wells, M. L. & Mayer, L. M. *Deep Sea Res.* (in the press).
10. Millero, F. J. & Sotolongo, S. *Geochim. cosmochim. Acta* **53**, 1867–1873 (1989).
11. Donard, O. F. X. *et al. Mar. Chem.* **27**, 117–136 (1989).
12. Wells, M. L. & Mayer, L. M. *Mar. Chem.* **32**, 195–210 (1991).
13. Zafiriou, O. C. & Dister, B. *J. geophys. Res.* **96**, 4939–4945 (1991).
14. O'Sullivan, D., Hanson, A., Miller, B. & Kester, D. *Limnol. Oceanogr.* (in the press).
15. Wang, M. K. & Hsu, P. H. *Soil Sci. Soc. Am. J.* **44**, 1089–1095 (1980).
16. Heller, H. G. & Langan, J. R. *J. chem. Soc. Perkin II*, 341–343 (1981).
17. Gast, P. R., Jursa, A. S., Castelli, J., Basu, S. & Aarons, J. *Handbook of Geophysics and Space Environments* (ed. Valley, S. L.) 16.1–16.38 (Air Force Cambridge Research Laboratory, Office of Aerospace Research, 1965).
18. Smith, R. C. & Baker, K. S. *Appl. Opt.* **20**, 177–184 (1981).
19. Bricaud, A., Morel, A. & Prieur, L. *Limnol. Oceanogr.* **26**, 43–53 (1981).
20. Kirk, J. T. O. *Geophys. Res.* **93**, 10897–10908 (1988).

ACKNOWLEDGEMENTS. We thank A. Monaco and R. Lesclaux for hospitality, M. Ewald for the Antarctic seawater sample, A. Dickson for helpful comments, and the CNRS ECOMARGE and EUROTRAC programs and the Center for Marine Studies, University of Maine, for funding this research.

An automaton for fractal patterns of fragmentation

Sandra J. Steacy & Charles G. Sammis

Department of Geological Sciences, University of Southern California, Los Angeles, California 90089–0740, USA

FRACTURES in the Earth's crust have a fractal structure over a wide range of length scales. A micromechanical model has been proposed¹ for the formation of fractal patterns of fragmentation in fault zones, based on the preferential fracture, at all length scales, of neighbours of a particle that have the same size as the particle itself. Here we explore this model in two and three dimensions using computer automata which implement these nearest-neighbour fracture rules. The automata produce random fractals which have capacity dimensions between 1.1 and 1.7 in two dimensions, and between 2.0 and 2.8 in three dimensions, the precise value depending on the packing geometry and the presence of long-range interactions imposed by uniform strain conditions. The fractal fragmentation patterns observed in natural systems tend to have dimensions between 2.5 and 2.7; we suggest that our model may permit an interpretation of these values in terms of the packing configuration (number of nearest neighbours) of the constituent particles.

Sammis *et al.*¹ showed that gouge from the Lopez Canyon fault zone in southern California was self-similar in the size range 10 μm to 1 cm with a fractal dimension $d_f = 1.6$ (in three-dimensional (3D) section, 2.6 for the corresponding three-dimensional (3D) isotropic random fractal). Barton and Hsieh² and Barton³ mapped 2-D fracture patterns on outcrops in the Nevada test site and found that they were fractal over scale ranges from centimetres to tens of metres with an average fractal dimension of 1.67 ± 0.07 .

Two processes that produce fractal fracture structures have been proposed, one related to the formation and growth of faults and the other to fragmentation in a previously granulated material. Both have been simulated in the laboratory. The growth

of shear fractures has been studied by Davy *et al.*⁴. They simulated the India-Asia continental collision by the slow advance of a rectangular indenter through a layer of cohesionless sand floating on a viscous substratum of silicone putty. The 2D pattern of conjugate shear fractures formed was found to be fractal with $d_f = 1.70 \pm 0.05$, independent of the viscosity of the substrate. Sornette *et al.*⁵ proposed that these patterns are the result of random crack growth in a critically loaded system, which is controlled by long-range screening and growth enhancement interactions between the growing fractures. In their model, entire domains of the crust are loaded to a critical state in an extension of the self-organized critical fault model of Bak and Tang⁶ to regional faulting patterns.

The development of a fractal fragmentation has been investigated by Biegel *et al.*⁷. They deformed a layer of initially uniformly sized fragments in simple shear and observed that the

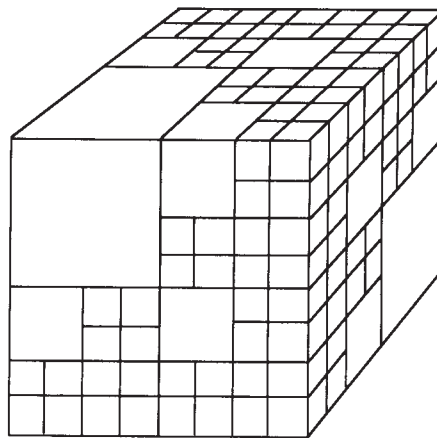


FIG. 1 Fractal cube. This figure has six blocks of edge length $1/2$ for every block of length 1, corresponding to a fractal dimension $d_f = \log 6 / \log 2 = 2.58$. The pattern has the property that no neighbours are the same size at any scale.